Received: 12 February 2022 | Revised: 23 April 2022 | Accepted: 23 April 2022

DOI: 10.1002/jrs.6366

RESEARCH ARTICLE

Journal of RAMAN SPECTROSCOPY WILEY

Combining Raman spectroscopy and synchrotron X-ray diffraction to unveil the order types in $A_3CaNb_2O_9$ (A = Ba, Sr) complex perovskites

João Elias F. S. Rodrigues[1,2] | Renilton C. Costa[3] | Paulo S. Pizani[4] | Antonio C. Hernandes[5] | José A. Alonso[2]

[1]European Synchrotron Radiation Facility (ESRF), Grenoble, France

[2]Instituto de Ciencia de Materiales de Madrid, CSIC, Madrid, Spain

[3]Department of Environmental Engineering, Federal University of Campina Grande, Pombal, Brazil

[4]Optical Spectroscopy and Raman Scattering Research Group, Federal University of São Carlos, São Carlos, Brazil

[5]São Carlos Institute of Physics, University of São Paulo, São Carlos, Brazil

Correspondence
João Elias F. S. Rodrigues, Instituto de Ciencia de Materiales de Madrid, CSIC, Cantoblanco, Madrid E-28049, Spain.
Email: rodrigues.joaoelias@gmail.com and rodrigues.joaoelias@esrf.fr

Funding information
Ministerio de Ciencia e Innovación, Grant/Award Number: MAT2017-84496-R; Spanish Ministry of Science, Innovation, and Universities; FAPESP, Grant/Award Number: 13/07793-6

Abstract

The structural ordering process in complex perovskites has a pivotal role for tuning many physical properties for broad applications, ranging from microwave technology, proton-conduction, multiferroicity, and so on. Therefore, the characterization of order type in these materials is essential for designing new devices with high-performance. Here, the coexistence of B-site 1:1 and 1:2 order types in mixed ordered $A_3CaNb_2O_9$ (A = Ba, Sr) perovskite was investigated by combining Raman spectroscopy and high-resolution synchrotron X-ray powder diffraction. High-wavenumber interval 700–825 cm^{-1} exhibits two bands concerning the symmetric breathing modes of [NbO_6] octahedra in $A_3CaNb_2O_9$, which were ascribed to the 1:1 and 1:2 domain regions in coexistence. This model was fully corroborated using two phases for describing the synchrotron X-ray pattern of the $Ba_3CaNb_2O_9$ sample. Therefore, the Raman spectroscopy can be indeed applied as a rapid tool for probing the achievement of ordered, partially ordered, or disordered structures in complex perovskites. For the first time, $BaLaCaNbO_6$ was synthesized and structural characterized, being indexed by the monoclinic unit cell belonging to the space group $I2/m$.

KEYWORDS

dielectric resonator, ordered perovskite, PC-SOFC, Raman scattering, synchrotron X-ray diffraction

1 | INTRODUCTION

The science and industry of microwave dielectric resonators have been, since their beginning, deeply affected by the development of high-performance ceramics based on ordered complex perovskites.[1,2] This led to great advances in communication technology (nowadays, the 5G-technology), which includes radar, mobile communications, global positioning system (GPS), Wi-Fi devices, and others.[3,4] Three main parameters are the key to optimize the resonator performance: a high dielectric permittivity (ε_r), which enables miniaturization; a high-Q_u, the unloaded quality factor; and near-zero temperature coefficient of resonant frequency (τ_f).[5] On the perovskites, a proper control of these parameters relies intensely on their crystal structure properties. Literature results have shown that the structural ordering process usually leads to an improved quality factor, which is desirable for microwave filters.[6–9] At the same time, tuning of the coefficient τ_f can be performed by octahedral tilting when the atomic radii at A-site are properly selected.[10,11]

The site ordering process in such perovskites has a crucial role not only for microwave applications but also for the proton-conduction in electrolytes,[12] multiferroicity,[13] and magnetism.[14] Both A- and B-sites are able to exhibit order with different topologies, such as rock salt (0-D), column (1-D), and layer (2-D).[15] The former is more stable than the others from an electrostatic point of view and is, therefore, the most common case.[16] An interesting example of 0-D topology comes from the B-site ordered $A_2B'B''O_6$, where B′ and B″ cations are distributed following the ratio –B′–B″–B′–B″–B′–B″– along the $[111]_c$ direction of the parental cubic cell. A very symmetric cubic space group (S.G. $Fm\bar{3}m$ or #225) describes its crystal structure, albeit symmetry lowering may occur due to the octahedral tilting.[17–19] Another important example is the B-site ordered $A_3B'B''_2O_9$ complex perovskite with the ionic distribution –B′–B″–B″–B′–B″–B″– along the $[111]_c$ direction, with a trigonal aristotype space group (S.G. $P\bar{3}m1$ or #164).[20,21] Those two complex systems are known as 1:1- and 1:2-type ordered perovskites, respectively, exhibiting potential applications in several fields ranging from multiferroicity to proton-conductor electrolytes.

A recent discussion in literature brought up the existence of a segregation between ordered domains in 1:2-type and an extra ordered structure at the grain boundaries, implying that different order types may coexist in the same material, that is, forming an average mixed ordered configuration.[8,22,23] For the 1:2 perovskites, a decrease in the 1:2 domain sizes combined with the appearance of domain boundaries usually damages the dielectric performance at microwave frequency, compromising their technological applicability. It is thus imperative to develop new methods for quickly identifying order types on such materials. In view of this challenge, we have investigated the capabilities of Raman scattering and high-angular resolution synchrotron X-ray powder diffraction (XRD) to unveil both 1:1 and 1:2 domain regions and their coexistence in $A_3CaNb_2O_9$ (A = Ba, Sr) mixed ordered systems and in their non-stoichiometric variation with calcium excess. These systems are promising for both microwave applications and as electrolytes in proton conducting solid oxide fuel cells (PC-SOFCs).[24,25] For the first time, a 1:1 ordered $BaLaCaNbO_6$ perovskite was synthesized and properly described by Raman spectroscopy and synchrotron XRD.

2 | METHODS

2.1 | Synthesis

Ceramic pieces of all the examined perovskite compounds were prepared from powders obtained by conventional solid-state reaction method, in which the reactants of $BaCO_3$ (99.80%, Alfa-Aesar), $SrCO_3$ (99.90%, Sigma-Aldrich), $CaCO_3$ (99.95%, Alfa-Aesar), La_2O_3 (99.99%, Alfa-Aesar), and Nb_2O_5 (99.90%, CBMM-Araxá) were used as metal sources. These reactants were weighted and, then, homogenized in nylon jar using isopropyl alcohol and zirconia balls. All the samples investigated here are summarized in Table 1. More details on the synthesis can be found in Rodrigues et al.[25] for $Ba_3CaNb_2O_9$, in Rodrigues et al.[27] for $Sr_3CaNb_2O_9$, and in Francisco et al.[26] for $Ba_3Ca_{1.18}Nb_{1.82}O_{9-\delta}$. For $BaLaCaNbO_6$, the dry mixtures were thermally treated in air at 1573 K for 2 h, pressed into pellets by both uniaxial and isostatic cold pressing, and then sintered at 1773 K for 26 h. To our knowledge, this composition is reported here for the first time.

2.2 | Characterization

Crystal structure and phase purity were probed by laboratory XRD pattern using a Bruker D8 Advance, with Cu-K_α radiation (40 *k*V and 30 *m*A, $\lambda = 1.54053$ Å) and *LynxEye* rapid detector, over a 2θ-angular interval from 10° up to 100° with step size of 0.02° and step time of 6 s. The diffraction patterns were compared with structural data available at the Inorganic Crystal Structure Database (ICSD, FIZ Karlsruhe, and NIST). No trace of secondary phase was found in any of the samples investigated here. High-angular resolution synchrotron X-ray diffraction (SXRD) was performed in the beamline MSPD of the CELLS-ALBA Synchrotron (Barcelona, Spain).[28] The pattern was recorded in the high-resolution setup with an incident energy of 38.07 keV ($\lambda = 0.32566$ Å). The powder sample was placed in a glass capillary, which was rotating along the collection time to better average the diffracted signal. Laboratory XRD and SXRD data were evaluated by Rietveld refinement method using the *Fullprof* software.[29] The microstructures of both powders and ceramics were examined using an Inspect F50 field-emission scanning electron microscope (FEI, Netherlands) at 5 kV coupled to an Energy dispersive X-ray (EDS) spectrometer, as summarized in Supporting Information.

Raman spectra at ambient condition were collected in a *HR*800 Evolution spectrometer from Horiba Jobin-Yvon, equipped with a Peltier-cooled charge-coupled device (CCD), 1800 gr mm^{-1} diffraction gratings, and Olympus microscope (50× objective LD, NA = 0.35). As an excitation source, an Nd:YAG laser operating at 532 nm was used in a *quasi*-backscattering geometry with a power below 1 mW. All the spectra were further corrected by the Bose–Einstein thermal factor prior to the

TABLE 1 List of ceramic samples investigated in this work together with their sintering conditions (i.e., temperature and time)

Sample	Abbreviation	Sint. temp. (K)	Sint. time (h)	Ref
$Ba_3CaNb_2O_9$	BCN	1863; 1773	2; 2–32	Rodrigues et al.[25]
$Ba_3Ca_{1.18}Nb_{1.82}O_{9-\delta}$	BCN18	1823	12	Francisco et al.[26]
$BaLaCaNbO_6$	BLCN	1773	26	This work
$Sr_3CaNb_2O_9$	SCN	1623; 1648; 1773	2; 2; 26	Rodrigues et al.[27]

fitting procedures by Lorentzian profiles (intensity, position, and linewidth) within the software *PeakFit*.[30]

Electrical characterizations were performed by means of impedance spectroscopy using a Solartron frequency response analyzer (model 1260) coupled with a dielectric interface model 1296, at a frequency range between 0.5 Hz and 1 MHz. For such measurements, ceramic pellets' polished surfaces were carefully painted with platinum paste in order to form parallel plate capacitors. The *ac* amplitude was defined after signal-to-noise ratio tests to ensure the results within Ohmic regime. The spectral data were adjusted using the software *ZView* 2.9c.[31] Details on the electrical studies in the aforementioned ceramics are presented in Supporting Information.

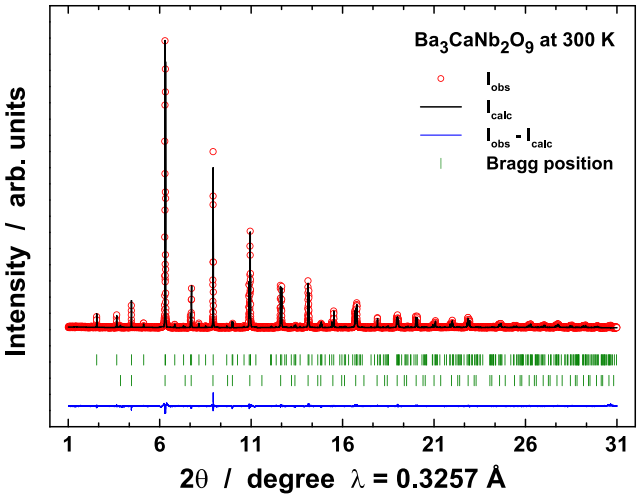

FIGURE 1 Rietveld plot of the structural refinement at room condition from synchrotron X-ray diffraction (SXRD) data of $Ba_3CaNb_2O_9$ sintered at 1773 K during 32 h. Observed (open symbol), calculated (black full line), their difference (blue line), and Bragg peaks (green vertical bars) [Colour figure can be viewed at wileyonlinelibrary.com]

3 | RESULTS AND DISCUSSION

3.1 | $Ba_3CaNb_2O_9$

In order to better investigate the coexistence of ordered regions, we have performed high-resolution synchrotron XRD study at room temperature in the $Ba_3CaNb_2O_9$ sample sintered at 1773 K for 32 h, as drawn in Figure 1. The use of high-resolution configuration was essential to unveil the ordered domains and to establish a valid structural model. First attempts of refinement considered one phase of trigonal BCN (S.G. $P\bar{3}m1$ or #164), which were unsatisfactory for accounting some additional diffraction peaks. A second model used a partial occupancy of Ca^{2+} and Nb^{5+} ions in their own sites (i.e., anti-site disorder), as proposed by Moreira and Dias for the trigonal $Ba_3MgNb_2O_9$.[32] In such a case, we hypothesized two different calcium (niobium) ions at 1*a* (2*d*), which lead to an occupational disorder at both Wyckoff sites. However, unsatisfactory refinements were also obtained. Then, we have started to consider a coexistence of two crystal structures: (i) a trigonal one with the 1:2 stacking sequence of –Ca–Nb–Nb–Ca–Nb–Nb– along *c*-axis; (ii) a cubic in which the Nb ions at 4*b* intercalate with a mixture of Ca (66.7%) and Nb (33.3%) at 4*a* in a 1:1 sequence along $[111]_c$ cubic direction. As a result, better reliability factors were obtained, and the extra diffraction peaks were successfully described by the cubic phase. Table 2 summarizes the atomic site distribution for both crystal structures under consideration. In the 32 h BCN sample, the phase percentage was estimated as 90.3(4)% and 9.7 (1)% for the trigonal and cubic phases, respectively. Both crystal structure representations are displayed in Figure S1.

Indeed, these cubic domains are undesired in $A_3B'B''_2O_9$ microwave compounds due to the occupational disorder at 4*a* sites, which normally leads to decreased quality factors and reduced device performance. On the other hand, such a coexistence would be promising for proton conductors, as for instance $Ba_3Ca_{1.18}Nb_{1.82}O_{9-\delta}$. Here, the calcium excess promotes the proton conductivity through a percolation process along $[NbO_6]$ octahedra.[33,34] In this way, BCN ceramics were sintered at 1773 K for different sintering times to promote a distinct distribution of phase percentages (between cubic and trigonal). As reported in recent literature,[22,35,36] the ordered domains in 1:2-type ordered perovskites proved to be quite sensitive to sintering conditions, including sintering temperature and time, annealing, and quench processes. Figure 2 displays

Space group		$P\bar{3}m1$		Fract. (%)	90.3(4)	
Atom	**Site**	***x***	***y***	***z***	**SOF**	**U (Å^2)**
Ba1	1*a*	0.0	0.0	0.0	1	0.025
Ba2	2*d*	0.3333	0.6667	0.6740(5)	1	0.004
Ca1	1*b*	0.0	0.0	0.5	1	0.003
Nb1	2*d*	0.3333	0.6667	0.1660	1	0.011
O1	6*i*	0.1729(8)	0.8269(4)	0.3190(5)	1	0.021
O2	3*e*	0.5	0.0	0.0	1	0.015
a (Å)	5.9029(3)	*c* (Å)	7.284(1)	*V* (Å^3)	219.80(4)	
R_{Bragg} (%)	5.94	R_f (%)	11.1	ρ (g cm^{-3})	5.907	
Space group		***Fm$\bar{3}$m***		**Fract. (%)**	**9.7(1)**	
Atom	**Site**	***x***	***y***	***z***	**SOF**	**U (Å^2)**
Ba	8*c*	0.25	0.25	0.25	1	0.011
Ca1	4*a*	0.0	0.0	0.0	0.667	0.011
Nb2	4*a*	0.0	0.0	0.0	0.333	0.011
Nb1	4*b*	0.5	0.5	0.5	1	0.011
O1	24*e*	0.2550(2)	0.0	0.0	1	0.024
a (Å)	8.3801(6)			*V* (Å^3)	588.51(4)	
R_{Bragg} (%)	6.28	R_f (%)	9.52	ρ (g cm^{-3})	5.883	

TABLE 2 Structural parameters for $Ba_3CaNb_2O_9$ sintered at 1773 K during 32 h refined from high-resolution synchrotron X-ray diffraction data at room condition

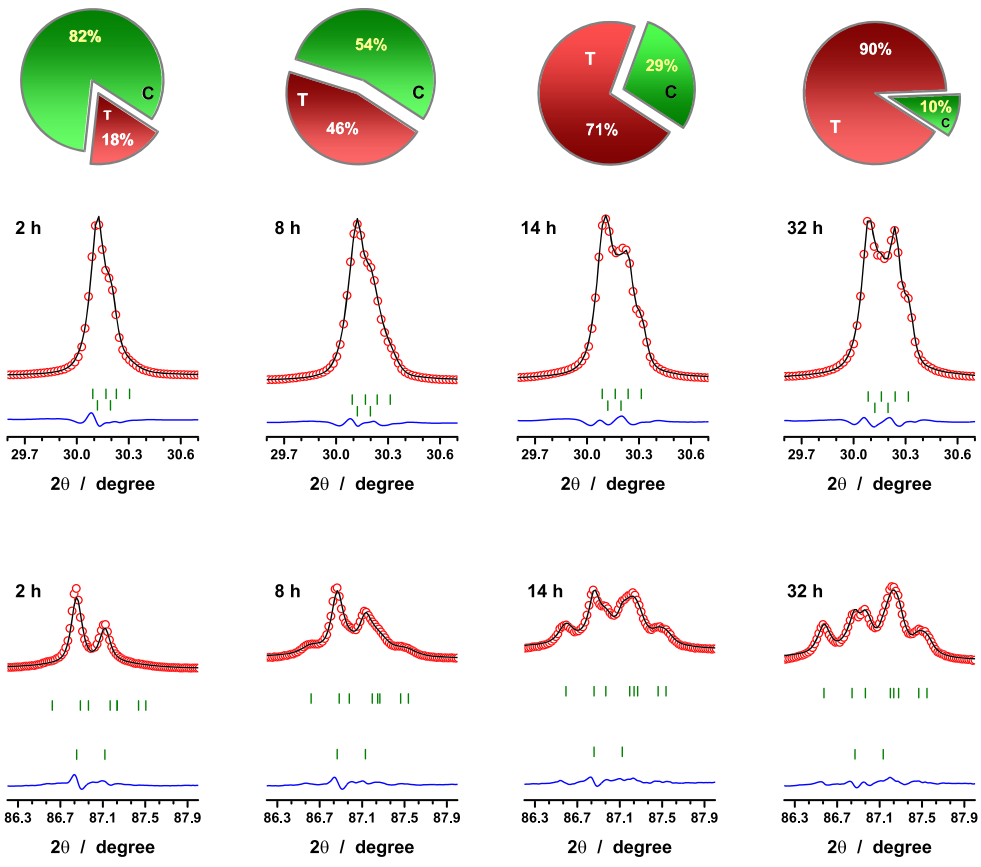

FIGURE 2 Rietveld plots at selected 2θ angular ranges to elucidate the transition from cubic (C) to trigonal (T) phase in $Ba_3CaNb_2O_9$ perovskite by varying the sintering time (2, 8, 14, and 32 h) [Colour figure can be viewed at wileyonlinelibrary.com]

some isolated laboratory X-ray diffraction peaks for the BCN sintered for 2, 8, 14, and 32 h. The full Rietveld refined patterns are available in the Supporting Information. The phase coexistence model (or mixed ordered structural model) in Figure 1 was applied to refine the structure from the X-ray data of Figure 2. We should mention the features of the main peak at $2\theta \sim 30.2°$, which was gradually splitted as sintering time increases. This event represents the transition from the cubic structure to the trigonal phase, although with some cubic phase residue (i.e., an incomplete transition). The distribution of both cubic and trigonal phases with sintering time is listed in Figure S2. In particular, the 2 h BCN sample displayed 17.6(6)% and 82(1)% of trigonal and cubic phases, respectively.

At the same time, Raman spectra of $Ba_3CaNb_2O_9$ were acquired at room temperature for characterizing the most symmetric modes, which concern the [NbO_6] stretching-type vibrations.[37] Details on the group-theory calculations, density functional theory (DFT)-derived vibrational, and experimental modes can be found elsewhere.[9,37,38] The goal here is to correlate the main features of high-wavenumber Raman modes with the phase percentage extracted from the Rietveld refinement. Figure 3a shows the Raman spectra of BCN ceramics sintered at 1773 K for 14 and 32 h. The modes in the most trigonal BCN sample (32 h) are in excellent agreement with previous investigations.[39,40] All the nine Raman active bands ($\Gamma_R = 4\boldsymbol{A}_{1g} \bigoplus 5\boldsymbol{E}_g$) predicted for the trigonal $P\bar{3}m1$ phase are clearly identified,[25] while a shoulder at 762–777 cm^{-1} of the main band near 810–820 cm^{-1} appeared in the spectra of the most cubic sample (14 h). For the cubic $Fm\bar{3}m$ structure, however, four modes ($\Gamma_R = 2\boldsymbol{F}_{2g} \bigoplus \boldsymbol{E}_g \bigoplus \boldsymbol{A}_{1g}$) are foreseen. Because the 14 h BCN ceramic has 71.4(7)% and 28.6(5)% of trigonal and cubic phases, respectively, it would be expected a predominance of trigonal modes, besides some residual signals from cubic phase.

We have evaluated the behavior of the Raman bands at 760–820 cm^{-1} as a function the phase concentration. The ratio $R_T = I_T/(I_T + I_C)$ is a simple quantification based on the Raman intensities, as exemplified in Figure 3b for BCN sintered at 1773 K for 14 h. In Figure 3c, one may see that a near-linear tendency between the trigonal phase concentration and the ratio R_T is observed up to 75% (of trigonal phase), when a change in slope is established above it. Above ~80% of trigonal phase, the quantification using Raman data starts to become difficult in view of the slight slope in R_T versus trigonal phase concentration curve. However, this result is enough to conclude that the phase concentration in $A_3CaNb_2O_9$ perovskites can be qualitatively followed

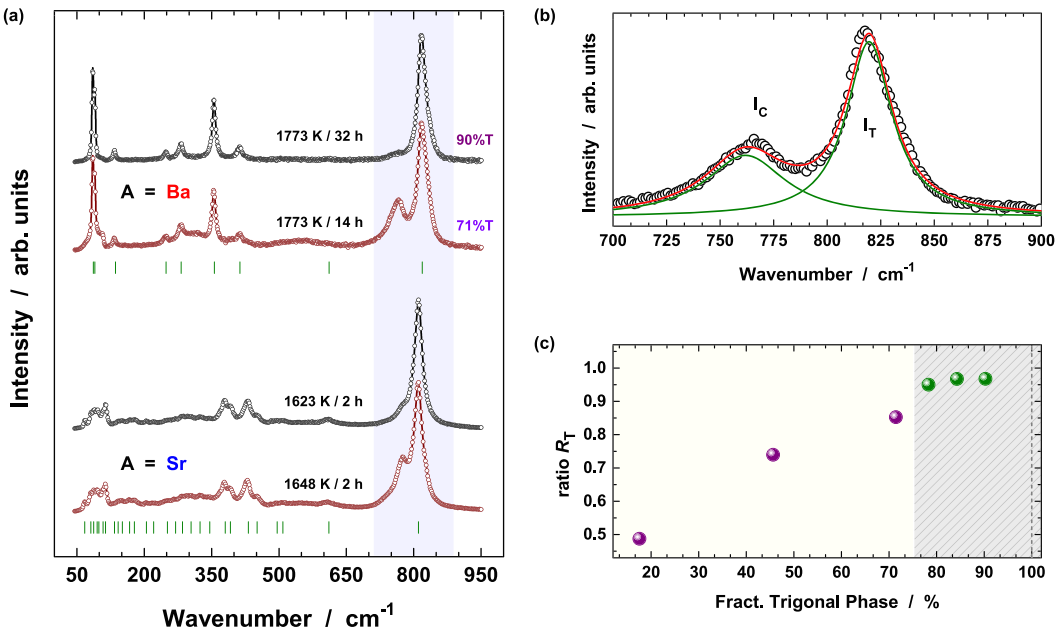

FIGURE 3 (a) Room temperature Raman spectra of $A_3CaNb_2O_9$ perovskite (A = Ba, Sr) at different sintering conditions. (b) Peak decomposition of the Raman bands at 760–820 cm^{-1} for BCN sintered at 1773 K for 14 h. (c) The ratio R_T versus trigonal phase concentration extracted from the Rietveld analysis of BCN series at 1773 K sintered for 2–32 h. Abbreviation: ratio $R_T = I_T/(I_T + I_C)$ [Colour figure can be viewed at wileyonlinelibrary.com]

using Raman spectroscopy as a tool for quick inspection. This result has important consequences for using the Raman technique as a quality control tool during the manufacturing of novel niobate-based microwave ceramics.

3.2 | $Sr_3CaNb_2O_9$

In Figure 3a, the Raman spectra of $Sr_3CaNb_2O_9$ perovskite are also represented, as synthesized at 1623 and 1648 K for 2 h. Different from A = Ba, the strontium-bearing sample has octahedral tilting, which lowers the crystal symmetry.[18,27,41] We have confirmed our previous work in which only 28 modes were detected at room condition, in contrast with the 42 predicted Raman-active modes ($\Gamma_R = 25\boldsymbol{A}_g \bigoplus 17\boldsymbol{B}_g$) for its $A2/m$ monoclinic phase.[27] Besides, the recurrent shoulder peak at 775 cm^{-1} suggests the presence of the 1:1 ordered domains, as it appeared for $Ba_3CaNb_2O_9$. The intensity of this peak has also changed with the sintering temperature in SCN sample. Different sintering conditions may induce variations in the intensity, position, and linewidth of the shoulder peak, including temperature or time during the synthesis procedures and possibly non-stoichiometry.[40] Therefore, such a topic deserves a special attention and better discussion.

In literature, Azough et al. obtained high-Q_u values for $Ba_3MgTa_2O_9$ compounds, after a long-time sintering, which were attributed to the reduction of the internal domain boundaries and, then, leading to the mono-domain grains.[8] Ma et al. correlated the low-Q_u values in $Ba_3(Co,Zn,Mg)Nb_2O_9$-doped with $BaZrO_3$ to 1:1 and 1:2 nanometer-sized ordered domains.[42] It seems that the domain boundaries with extra ordered structure, that is, type 1:1, acts as extrinsic damping factor for the microwave signal transmitted through the resonator device.[43] Although the domain boundaries are undesired for dielectric ceramics, they constitute a key element in proton-conductor electrolytes based on complex perovskites due to their role in increasing the effective mobility and, hence, the macroscopic conductivity.[24,44] In the last case, Colomban et al. demonstrated that the maximal water uptake within the crystal lattice depends on the cation/oxygen disorder.[45] For $Ba_3CaNb_2O_9$, as a case of study, the dielectric loss (i.e., $\tan\delta \approx Q_u^{-1}$) tends to decrease as the crystal structure approaches a trigonal unit cell with 1:2 B-site order between Ca^{2+} and Nb^{5+} cations.[9] In this example, the Raman intensity of a shoulder peak at ~760 cm^{-1} almost vanishes when the dielectric resonator presents a low dielectric loss at microwave range, corroborating the results of Azough et al. for the isostructural $Ba_3MgTa_2O_9$ perovskite.

3.3 | $BaLaCaNbO_6$

In order to better understand the Raman signature of mixed ordered domain regions in $A_3CaNb_2O_9$ complex perovskite, a 1:1 ordered composition containing Ca^{2+} and Nb^{5+} ions at B-site was synthesized with the chemical formula $BaLaCaNbO_6$. We employed high-resolution SXRD data to describe its crystal structure, as drawn in Figure 4a. Different from the expected, the aristotype cubic $Fm\bar{3}m$ space group was not suitable to describe the peak distribution. Then, Raman spectroscopy was essential to provide further clues on its unit-cell symmetry. Its full Raman spectrum is shown in Figure 4b. In a first inspection, one can clearly see four Raman modes at ~117, 415, 505, and 756 cm^{-1} that agree with group-theory predictions for the cubic $m\bar{3}m$ factor group, that is, $\Gamma_R = 2\boldsymbol{F}_{2g} \bigoplus \boldsymbol{E}_g \bigoplus \boldsymbol{A}_{1g}$.[46] Nevertheless, more five modes could be clearly identified, which was an evidence for the symmetry lowering process. Indeed, the incorporation of La^{3+} (r = 1.36 Å, CN = 12) ions at Ba^{2+} sites

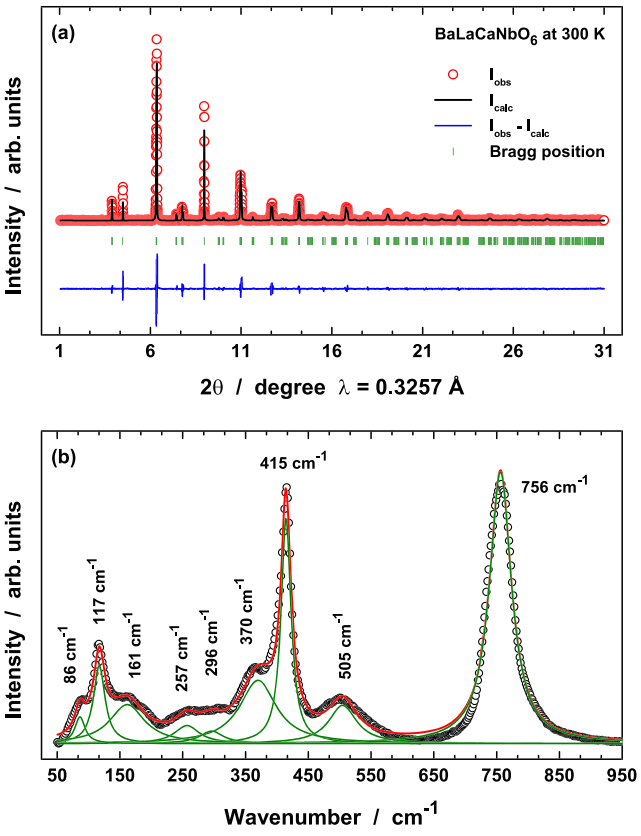

FIGURE 4 (a) Rietveld plot of the structural refinement at room condition from synchrotron X-ray diffraction (SXRD) data of $BaLaCaNbO_6$ sintered at 1773 K during 26 h. Observed (open symbol), calculated (black full line), their difference (blue line), and Bragg peaks (green vertical bars). (b) Raman spectrum of $BaLaCaNbO_6$ perovskite at room condition [Colour figure can be viewed at wileyonlinelibrary.com]

($r = 1.61$ Å, CN = 12) may promote structural instabilities, which may induce the octahedral tilting mechanism.

After a detailed literature revision,[18,47] we have concluded that the most plausible space group to index the BLCN unit cell is the monoclinic $I2/m$ (S.G. #12), being derived from the aristotype cubic phase $Fm\bar{3}m$ through an out-of-phase tilting as represented by the Glazer system $a^0b^-b^-$.[17] Such assumption was also confirmed by the software SPuDS.[48] The structural details are summarized in Table 3 together with the vibrational modes predictions using the group theory on the factor group $2/m$. The monoclinic structure of BLCN is displayed in Figure S1. Initial refinements started from the isostructural compound Ba_2SrWO_6,[49] which also has similar Raman distribution with 12 Raman-active modes at ambient condition.[47] For BLCN, instead, only nine Raman peaks were used to fit its room condition spectrum in Figure 4b. This perovskite has indeed a pseudo-cubic crystal structure,[50] in which Ca^{2+} and Nb^{5+} ions follow the 1:1 order. Special attention should be given to most symmetric Raman mode located at 756 cm^{-1}: it represents a breathing-type mode of [NbO_6] octahedra.[51]

In Figure 5a, we compared the high-wavenumber Raman spectrum of $BaLaCaNbO_6$ with those recorded in mixed ordered $A_3CaNb_2O_9$ (A = Ba, Sr) perovskites (i.e., selected samples with minor cubic content). The shoulder band at 762–777 cm^{-1} is tentatively assigned as a

TABLE 3 Structural parameters for $BaLaCaNbO_6$ sintered at 1773 K for 26 h refined from high-resolution synchrotron X-ray diffraction data at room condition

Space group		$I2/m$			
Atom	**Site**	***x***	***y***	***z***	**Irreducible representation**
Ba/La	4*i*	0.5050	0.5	0.2507	$2\boldsymbol{A}_g \oplus \boldsymbol{A}_u \oplus \boldsymbol{B}_g \oplus 2\boldsymbol{B}_u$
Ca	2*b*	0.0	0.5	0.0	$\boldsymbol{A}_u \oplus 2\boldsymbol{B}_u$
Nb	2*c*	0.5	0.0	0.0	$\boldsymbol{A}_u \oplus 2\boldsymbol{B}_u$
O1	4*i*	0.5566	0.0	0.2560	$2\boldsymbol{A}_g \oplus \boldsymbol{A}_u \oplus \boldsymbol{B}_g \oplus 2\boldsymbol{B}_u$
O2	8*j*	0.2672	0.1687	0.0351	$3\boldsymbol{A}_g \oplus 3\boldsymbol{A}_u \oplus 3\boldsymbol{B}_g \oplus 3\boldsymbol{B}_u$
a (Å)	5.8883(3)			Γ_{Total}	$7\boldsymbol{A}_g \oplus 7\boldsymbol{A}_u \oplus 5\boldsymbol{B}_g \oplus 11\boldsymbol{B}_u$
b (Å)	5.8970(3)			$\Gamma_{Acoustic}$	$\boldsymbol{A}_u \oplus 2\boldsymbol{B}_u$
c (Å)	8.3376(4)			Γ_{Silent}	0
β (°)	90.504(2)			$\Gamma_{Infrared}$	$6\boldsymbol{A}_u \oplus 9\boldsymbol{B}_u$
R_{Bragg} (%)	8.40			Γ_{Raman}	$7\boldsymbol{A}_g \oplus 5\boldsymbol{B}_g$
R_f (%)	5.39				

Note: Nuclear site group analysis for the monoclinic structure belonging to the space group $I2/m$ is also summarized.

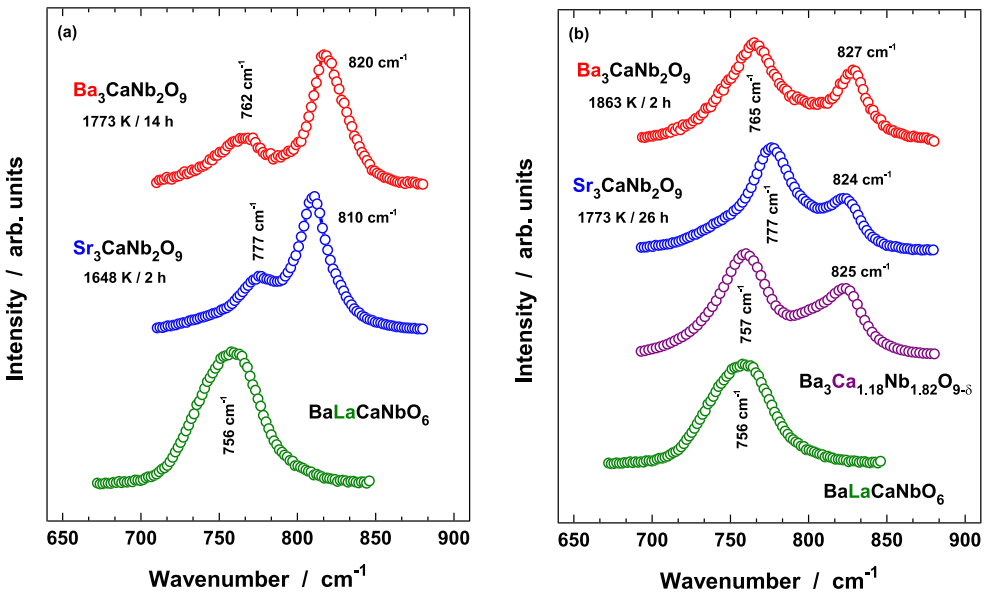

FIGURE 5 (a) High-wavenumber Raman spectra, at room temperature, of mixed ordered $A_3CaNb_2O_9$ (A = Ba, Sr) and $BaLaCaNbO_6$ ceramics. The comparison shows that the shoulder peak may be ascribed as a symmetry mode from the 1:1 Ca/Nb domain. (b) Raman spectra of $A_3CaNb_2O_9$ (with large amount of cubic phase), $Ba_3Ca_{1.18}Nb_{1.82}O_{9-\delta}$, and $BaLaCaNbO_6$ ceramics. From the comparison with the last sample, we have argued that there is a predominance of the 1:1-type order [Colour figure can be viewed at wileyonlinelibrary.com]

mode coming from regions in mixed ordered sample with 1:1 B-site domains. In this way, a coexistence of both order types (1:1 and 1:2) is allowed in a single ceramic grain, as seen from SXRD data. This hypothesis is indeed not so far from reality, because domain boundaries with different order types were already reported using high-resolution transmission electron microscopy.[22] Hence, the arrangements of [CaO_6] and [NbO_6] octahedra can be identified by following the high-wavenumber Raman modes at 700–825 cm^{-1}. From our results, the mode at 762–777 cm^{-1} is definitively related to 1:1 Ca/Nb ordering, whereas the one centered near 810–820 cm^{-1} concerns the signature of 1:2 Ca/Nb ordering.

This difference in vibrational energies of 1:1 and 1:2 related modes was explained by Blasse et al. by considering two different local surroundings for the [NbO_6] octahedra.[52] In the 1:1 ordered cubic structure, the Nb^{5+} ions are at $m\bar{3}m$ sites; whereas in the 1:2 ordered structure, these ions are at 3*m* sites for $Ba_3CaNb_2O_9$. Such differences in local site symmetry explain the vibrational responses coming from the domains with different order types at B-site. This result has a significant practical consequence, because it allows the monitoring of one or both types of order by Raman spectroscopy, which is important for guiding a correct choice of the material composition and preparation for applications.

Figure 5b displays the high-wavenumber part of the Raman spectrum of $BaLaCaNbO_6$ with those acquired in highly cubic $A_3CaNb_2O_9$ (A: Ba, 1863 K for 2 h; Sr, 1773 K for 26 h) perovskites. Here, the sintering conditions of those ceramics were chosen by changing temperature/time and, at the same time, checking the Raman intensities at 765–777 cm^{-1}. We have selected sintering parameters to provide $A_3CaNb_2O_9$ samples with large amounts of the cubic phase. Figure 5b also presents the Raman spectrum of $Ba_3Ca_{1.18}Nb_{1.82}O_{9-\delta}$ ceramic, which is a well-known proton conductor applicable as an electrolyte for PC-SOFCs.[12] One may see the occurrence of a more intense band at 757–777 cm^{-1} in comparison with that at 824–827 cm^{-1}. This result denotes that there is a coexistence of the two order types with a preferential tendency for the 1:1-type in BCN18, being the 1:2-type a minor phase. As reported by Du and Nowick,[44] this condition is sufficient to enhance the conductivity explained in view of the percolation theory. The high-performance of $Ba_3Ca_{1.18}Nb_{1.82}O_{9-\delta}$ electrolytes is due to inhomogeneity of the proton distribution in both ordered regions.

4 | CONCLUSION

In this paper, we have investigated the Raman spectra of complex perovskites and their nonstoichiometric variations in order to clarify the occurrence of different order types as induced by thermal treatments. Indeed, high-angular synchrotron XRD unveiled the coexistence of two order-types in mixed ordered $A_3CaNb_2O_9$ (A = Ba, Sr), i.e., 1:1 Ca/Nb (cubic) and 1:2 Ca/Nb (trigonal). The high-wavenumber region of Raman spectra exhibited two symmetric modes (two-mode behavior) at 700–825 cm^{-1}. For the first time, the cubic $BaLaCaNbO_6$-based perovskite was synthesized and its cell indexed to the monoclinic space group $I2/m$, which helped us to assign the shoulder peak at 757–777 cm^{-1} and the main band at 810–827 cm^{-1}. We have argued that these two modes are fingerprints of coexisting 1:1 and 1:2 ordered domains, respectively, corroborating the SXRD data. Our result has consequences for using the Raman technique as a quality control tool during the preparation of niobate-based microwave ceramics.

ACKNOWLEDGEMENTS

Financial support from the Brazilian agencies FAPESP (Grant number: 13/07793-6) is gratefully acknowledged. J.A.A. thanks the Spanish Ministry of Science, Innovation, and Universities for funding the project MAT2017-84496-R. We thank the CELLS-ALBA (Spain) for making all the facilities available for the synchrotron radiation experiments.

ORCID

João Elias F. S. Rodrigues https://orcid.org/0000-0002-9220-5809
Renilton C. Costa https://orcid.org/0000-0003-2129-2930
Paulo S. Pizani https://orcid.org/0000-0002-5914-1671
Antonio C. Hernandes https://orcid.org/0000-0002-7556-8050
José A. Alonso https://orcid.org/0000-0001-5329-1225

REFERENCES

[1] M. Sebastian, *Dielectric Materials for Wireless Communication*, 1st ed., Elsevier, Amsterdam **2008**.
[2] M. T. Sebastian, R. Ubic, H. Jantunen, *Int. Mater. Rev.* **2015**, *60*, 392.
[3] P. Mohanan, S. Mridula, *Microwave Materials and Applications 2V Set*, John Wiley & Sons, Ltd, Chichester, UK **2017** 683.
[4] T. A. Vanderah, *Science* **2002**, *298*, 1182.
[5] H. Hughes, D. M. Iddles, I. M. Reaney, *Appl. Phys. Lett.* **2001**, *79*, 2952.
[6] S. B. Desu, H. M. O'Bryan, *J. Am. Ceram. Soc.* **1985**, *68*, 546.
[7] A. Dias, R. L. Moreira, *J. Appl. Phys.* **2003**, *94*, 3414.
[8] F. Azough, R. Freer, D. Iddles, T. Shimada, B. Schaffer, *J. Eur. Ceram. Soc.* **2014**, *34*, 2285.
[9] J. E. F. S. Rodrigues, P. J. Castro, P. S. Pizani, W. R. Correr, A. C. Hernandes, *Ceram. Int.* **2016**, *42*, 18087.

[10] E. L. Colla, I. M. Reaney, N. Setter, *J. Appl. Phys.* **1993**, *74*, 3414.
[11] I. M. Reaney, E. L. Colla, N. Setter, *Jpn. J. Appl. Phys.* **1994**, *33*, 3984.
[12] K. Singh, W. H. Kan, B. Patton, A. Huq, V. Thangadurai, *Inorg. Chem.* **2018**, *57*, 2609.
[13] Y. Shimakawa, M. Azuma, N. Ichikawa, *Dent. Mater.* **2011**, *4*, 153.
[14] R. X. Silva, A. S. de Menezes, R. M. Almeida, R. L. Moreira, R. Paniago, X. Marti, H. Reichlova, M. Maryško, M. V. dos S. Rezende, C. W. A. Paschoal, *J. Alloys Compd.* **2016**, *661*, 541.
[15] S. Vasala, M. Karppinen, *Prog. J. Solid State Chem.* **2015**, *43*, 1.
[16] G. King, P. M. Woodward, *J. Mater. Chem.* **2010**, *20*, 5785.
[17] P. M. Woodward, *Acta Crystallogr. Sect. B Struct. Sci.* **1997**, *53*, 32.
[18] R. L. Andrews, A. M. Heyns, P. M. Woodward, *Dalton Trans.* **2015**, *44*, 10700.
[19] S. C. Lal, J. I. Naseemabeevi, S. Ganesanpotti, *Mater. Adv.* **2021**, *2*, 1328.
[20] C. J. Howard, H. T. Stokes, *Acta Crystallogr. B* **2004**, *60*, 674.
[21] F. Galasso, J. Pyle, *Inorg. Chem.* **1963**, *2*, 482.
[22] P. P. Ma, H. Gu, X. M. Chen, *J. Am. Ceram. Soc.* **2016**, *99*, 1299.
[23] P. P. Ma, H. Gu, X. M. Chen, *J. Mater. Chem. C* **2015**, *3*, 10755.
[24] S. Wang, Y. Chen, S. Fang, L. Zhang, M. Tang, K. An, K. S. Brinkman, F. Chen, *Chem. Mater.* **2014**, *2021*, 26.
[25] J. E. Rodrigues, D. M. Bezerra, A. C. Hernandes, *Ceram. Int.* **2017**, *43*, 14015.
[26] L. H. Francisco, J. E. Rodrigues, W. R. Correr, A. C. Hernandes, *Ceram. Int.* **2018**, *44*, 10806.
[27] J. E. Rodrigues, D. M. Bezerra, R. C. Costa, P. S. Pizani, A. C. Hernandes, *J. Raman Spectrosc.* **2017**, *48*, 1243.
[28] F. Fauth, R. Boer, F. Gil-Ortiz, C. Popescu, O. Vallcorba, I. Peral, D. Fullà, J. Benach, J. Juanhuix, *Eur. Phys. J. Plus.* **2015**, *130*, 160. https://doi.org/10.1140/epjp/i2015-15160-y
[29] J. Rodríguez-Carvajal, *Phys. B Phys. Condens. Matter* **1993**, *192*, 55.
[30] D. A. Long, *The Raman Effect: A Unified Treatment of the Theory of Raman Scattering by Molecules*, John Wiley & Sons, West Sussex, England **2002**.
[31] D. Johnson, *Software ZView 3.2*, Scribner Associates, Inc, Southern Pines **2009**.
[32] R. L. Moreira, F. M. Matinaga, A. Dias, *Appl. Phys. Lett.* **2001**, *78*, 428.
[33] A. S. Nowick, Y. Du, *Solid State Ionics* **1995**, *77*, 137.
[34] T. Schober, J. Friedrich, *J. Am. Ceram. Soc.* **2004**, *82*, 3125.
[35] P. P. Ma, X. M. Chen, *Mater. Charact.* **2019**, *158*, 109938.
[36] R. Da Shi, L. Liu, X. L. Zhu, X. M. Chen, *J. Am. Ceram. Soc.* **2022**, *105*, 1159.
[37] M. M. Ferrer, J. R. Sambrano, A. C. Hernandes, J. E. F. S. Rodrigues, *J. Raman Spectrosc.* **2020**, *51*, 1219. https://onlinelibrary.wiley.com/doi/abs/10.1002/jrs.5895
[38] J. E. F. S. Rodrigues, E. Moreira, D. M. Bezerra, A. P. Maciel, C. W. de Araujo Paschoal, *Mater. Res. Bull.* **2013**, *48*, 3298. https://doi.org/10.1016/j.materresbull.2013.05.005
[39] J. Deng, J. Chen, R. Yu, G. Liu, X. Xing, *J. Alloys Compd.* **2009**, *472*, 502.
[40] O. Valdez-Ramírez, F. Gómez-García, M. A. Camacho-López, E. Ruiz-Trejo, *J. Electroceram.* **2012**, *28*, 226.
[41] A. Dias, F. M. Matinaga, R. L. Moreira, *Chem. Mater.* **2007**, *19*, 2335.
[42] P. P. Ma, L. Yi, S. Y. Wu, X. M. Chen, H. Gu, *J. Am. Ceram. Soc.* **2015**, *98*, 520.
[43] J. E. F. S. Rodrigues, P. J. Castro, P. S. Pizani, W. R. Correr, A. C. Hernandes, *Ceram. Int.* **2016**, *42*, 18087.
[44] Y. Du, A. S. Nowick, *J. Am. Ceram. Soc.* **1995**, *78*, 3033.
[45] P. Colomban, F. Romain, A. Neiman, I. Animitsa, *Solid State Ionics* **2001**, *145*, 339.
[46] J. E. Rodrigues, D. M. Bezerra, A. C. Hernandes, *J. Raman Spectrosc.* **2018**, *1822*, 49.
[47] A. Dias, K. P. E. Siqueira, R. L. Moreira, *J. Raman Spectrosc.* **2010**, *41*, 93.
[48] M. W. Lufaso, P. M. Woodward, *Acta Crystallogr. Sect. B Struct. Sci.* **2001**, *57*, 725.
[49] W. T. Fu, Y. S. Au, S. Akerboom, D. J. W. IJdo, *J. Solid State Chem.* **2008**, *181*, 2523.
[50] Y. I. Kim, P. M. Woodward, *J. Solid State Chem.* **2007**, *180*, 2798.
[51] C.-L. Diao, C.-H. Wang, N.-N. Luo, Z.-M. Qi, T. Shao, Y.-Y. Wang, J. Lu, F. Shi, X.-P. Jing, *J. Am. Ceram. Soc.* **2013**, *96*, 2898.
[52] G. Blasse, A. F. Corsmit, *J. Solid State Chem.* **1974**, *10*, 39.

SUPPORTING INFORMATION

Additional supporting information may be found in the online version of the article at the publisher's website.

How to cite this article: J. E. F. S. Rodrigues, R. C. Costa, P. S. Pizani, A. C. Hernandes, J. A. Alonso, *J Raman Spectrosc* **2022**, *53*(7), 1333. https://doi.org/10.1002/jrs.6366